




Robust Control using a \mathcal{H}_∞ Mixed Sensitivity Approach for a UAV with a Suspended Payload

Jefferson A. Enriquez Quispe , Tito Y. Galarza Delgado , and Juan C. Cutipa Luque 

Abstract—Unmanned aerial vehicles (UAVs) are increasingly being utilized in a wide range of applications, including military operations, agronomy, and delivery services, among others. These applications often require load transportation missions which are executed by the UAV, that can be executed by the UAV, a link, and its payload. The UAV with its suspended load is a kind of highly coupled system where good performance and stability are required despite disturbances and model uncertainties. In this work, we present an \mathcal{H}_∞ robust control design for this system. The desired controller is synthesized to achieve suboptimal robustness in terms of performance and stability. Simulation results demonstrate robustness against disturbances and model uncertainties. In terms of performance, this control system shows up to a 50% reduction in load oscillations compared to alternative controllers, such as the Linear Quadratic Regulator (LQR).

Link to graphical and video abstracts, and to code:
<https://latam.ieeer9.org/index.php/transactions/article/view/9285>

Index Terms— \mathcal{H}_∞ , Kane equation, multibody dynamics, robust control, unmanned aerial vehicle.

I. INTRODUCTION

THERE is a growing interest in utilizing unmanned aerial vehicles (UAVs) across diverse fields, including military operations, security, agronomy, topography, electrical network inspection, emergency response, and hazardous tasks, among others [1]–[3]. Many of these applications require the transportation of a suspended load. For instance, in the agronomy industry, a UAV configuration with a suspended load is used to prevent damage to crops [4]. Similarly, such a configuration is employed for data collection using image processing in [5]. Other applications, such as tool transportation in emergency situations or in rugged terrain that limits human intervention, such as canyons, ravines, and mountainous or marine scenarios, are addressed in [6] and [7], where the UAV with suspended load system is exposed to environmental disturbances. Even in [8], the performance of the Linear Quadratic Regulator (LQR) controller was studied with a non-solid load.

Regarding modeling, an early study [9] presents the modeling of small helicopters with a suspended load using Kane's method. Subsequently, [10] presents the modeling of a UAV with payload using Kane's equations; this approach enables

the analysis of the UAV with the suspended payload system as an interconnected multibody system, thereby coupling the dynamics of both the UAV and the payload. Studies of UAV control systems employing a conventional controller synthesized solely from UAV dynamics demonstrate poor performance and tracking capabilities due to the oscillations of the suspended load and disturbances, such as sensor noise. These factors contribute to performance degradation and can even lead to system instability.

Regarding controllers for highly coupled systems, [10] presents a nonlinear controller with swing-damping aimed at reducing oscillations; however, this resulted in a lag effect in tracking performance. Furthermore, special consideration must be given to the system dynamics for control design. The controller can be synthesized using the complete system dynamics (UAV with suspended load) or by simplifying certain dynamics. However, the former approach generally provides superior performance and tracking [11].

Another proposal for a hybrid control strategy integrating artificial intelligence and feedback linearization, demonstrated high robustness [12]. In [13], the authors introduced stability improvements in stability through neural network control. However, this strategy requires high computational processing at the ground station, and the data link between the ground station and the UAV is maintained via a wireless connection. Consequently, communication delays can lead to degraded UAV performance [14].

In [15], a Model Reference Adaptive Control (MRAC) system is presented, noted for its robustness against uncertainties. The results are compared with those of a Proportional-Integral-Derivative (PID) controller applied to a UAV with a load oscillating along a single axis; however, no significant improvement in stability is observed with the MRAC controller.

Regarding robust control strategies, recent research [16], [17] presents a sliding mode control strategy based on neural networks. However, the results indicate excessive load oscillations, even when considering external disturbances. Other control approaches, such as Model Predictive Control (MPC) described in [18]–[20], employ a nonlinear MPC that significantly reduces load oscillation. Nevertheless, the development of specific robustness characteristics, such as sensor noise rejection, is not addressed.

In the context of robust control, [21] presents the Interconnection and Damping Assignment-Passivity Based Control (IDA-PBC) to achieve a desired Hamiltonian, enabling control of the UAV and attenuation of load oscillations when subjected to constant disturbances. However, it exhibits limitations with variable disturbances, which can potentially lead to instability.

The associate editor coordinating the review of this manuscript and approving it for publication was Pedro Machado de Almeida (*Corresponding author: Jefferson Abraham Enriquez Quispe*).

Jefferson A. Enriquez Quispe, T. Y. G. Delgado, and J. C. C. Luque, are with Universidad Nacional de San Agustín, Arequipa, Perú (e-mails: jenriquezqu@unsa.edu.pe, tgalarza@unsa.edu.pe, and jcutipalu@unsa.edu.pe)

A similar study [22] employs energy-based control (CBE) for translational dynamics, achieving attenuation of load oscillations, and a Linear Matrix Inequality (LMI)-based control for rotational dynamics, noting that the CBE control is sensitive to load position measurement.

An \mathcal{H}_∞ robust control approach applied to a single UAV (without suspended load) demonstrates superior performance in tracking and stability, even in the presence of disturbances and unmodeled dynamics, when compared to a geometric nonlinear PID controller [23]. In a subsequent study [24], a mixed $\mathcal{H}_2/\mathcal{H}_\infty$ controller is presented, applied to the Euler-Lagrange model of the UAV system with a suspended load, showing good performance. However, only the impact of additive disturbances is addressed. Following the same line of research, [25] employs the \mathcal{H}_∞ criterion, which minimizes the effects of disturbances, to demonstrate the stability of a proposed observer designed to reduce disturbances.

As previously noted, the modeling and control of UAV systems with a suspended payload have been addressed in the literature. However, the application of control based on the \mathcal{H}_∞ norm, which aims to reduce disturbance sensitivity and limit control efforts through weighting functions and a complementary function that enhances performance, has not yet been studied in the literature. This research proposes solutions to mitigate issues related to oscillations, disturbances, and parametric uncertainties through a linear robust control approach based on the \mathcal{H}_∞ norm applied to the dynamic model of the system, derived using Kane's method.

II. UAV MODEL

The UAV with suspended load constitutes a highly coupled system, and its dynamic model can be derived using either Newton's laws of motion or Lagrangian mechanics. In this work, the UAV model is represented by the following equations, which consider the North East Down (NED) frame $\{n\}$ and the Body-Fixed (BF) frame $\{b\}$ [26].

$$\dot{\mathbf{p}} = \mathbf{v}, \quad (1)$$

$$m_c \dot{\mathbf{v}} = m_c \mathbf{g} + \mathbf{R}(\Theta) \mathbf{f} + \mathbf{f}_e, \quad (2)$$

$$\dot{\Theta} = \mathbf{T}(\Theta) \boldsymbol{\omega}, \quad (3)$$

$$\mathbf{I} \dot{\boldsymbol{\omega}} = \mathbf{S}(\mathbf{I} \boldsymbol{\omega}) \boldsymbol{\omega} + \mathbf{M}, \quad (4)$$

where $\mathbf{p} \in \mathbb{R}^3$ is the position vector [m] in the frame $\{n\}$, $\mathbf{v} \in \mathbb{R}^3$ is the linear velocity [m/s] in $\{n\}$, m_c is the mass [kg] of the UAV, $\mathbf{g} = [0 \ 0 \ g]^T$ is the gravity vector with g as gravitational acceleration [m/s²], $\mathbf{R}(\Theta) \in SO(3)$ is the rotation matrix that transforms vectors from the $\{n\}$ to $\{b\}$. Here, $SO(3)$ denotes the special orthogonal group of all rotation matrices in three dimensions that preserve vector length and orientation. \mathbf{f} is a vertical thrust [N] acting along the z axis of $\{b\}$, \mathbf{f}_e represents the environmental forces [N], $\Theta = [\phi, \theta, \psi]^T$ is the attitude vector (roll, pitch, and yaw angles, respectively), $\boldsymbol{\omega}$ is the angular velocity vector [rad/s], \mathbf{I} is the inertia matrix [kg · m²] in $\{n\}$, $\mathbf{S}(\mathbf{I} \boldsymbol{\omega})$ is $\mathbf{I} \boldsymbol{\omega} \times \boldsymbol{\omega}$ where $\mathbf{S}(\ast)$ is the skew-symmetric transformation, \mathbf{M} are

the torques applied by the motors, and $\mathbf{T}(\Theta)$ is the frame transformation matrix defined as:

$$\mathbf{T}(\Theta) = \begin{bmatrix} 1 & \sin \phi \tan \theta & \cos \phi \tan \theta \\ 0 & \cos \phi & -\sin \phi \\ 0 & \frac{\sin \phi}{\cos \theta} & \frac{\cos \phi}{\cos \theta} \end{bmatrix}, \cos \theta \neq 0. \quad (5)$$

The modeling is subject to the following assumptions: The tether connecting the payload is attached to the UAV's center of gravity (CG), is considered rigid, and its mass and drag neglected. The payload is modeled as point-mass, and air drag is acting on it considered.

Given the highly coupled nature of the system, and the fact that the suspended load is attached to the UAV's center of mass, its primary effect will be on translational movements; rotational movements are considered negligible. Therefore, the load forces $\boldsymbol{\tau}_L$ should be included in (2), which relates to translational movement. The UAV dynamics to be considered are then:

$$\dot{\mathbf{p}} = \mathbf{v}, \quad (6)$$

$$m_c \dot{\mathbf{v}} = m_c \mathbf{g} + \mathbf{R}(\Theta) \mathbf{f} + \boldsymbol{\tau}_L + \mathbf{f}_e, \quad (7)$$

where $\mathbf{R}(\Theta) \mathbf{f} \in \mathbb{R}^3$ is a control force. In translational motions, it is possible to control the UAV considering at least the roll and pitch dynamics, which are included in $\mathbf{R}(\Theta)$ [27]. The suspended load can be considered a simple pendulum considering the CG of UAV as the oscillation point of the load [28]. As a similar assumption, this work considers the movement of the pendulum in the xz and yz planes as shown in Fig. 2, where ϕ_L is the angle resulting from the rotational movement in the x axis and θ_L is the rotational angle in the y axis. Thus, ϕ_L and θ_L describe the position of the suspended load.

The dynamic model of a UAV is highly nonlinear, becoming a highly coupled system when the model considers the dynamics of the suspended load. To model this system, it is necessary to use the Kane equations, which are used for modeling multibody systems [9]. Considering (6) and (7), a nonlinear model is obtained, thus representing the whole system using the Kane equations. [27]:

$$\dot{\boldsymbol{\eta}} = \boldsymbol{\nu}, \quad (8)$$

$$\dot{\boldsymbol{\nu}} = \mathbf{M}_{(\eta)}^*{}^{-1} (-\mathbf{C}_{(\eta, \nu)}^* \boldsymbol{\nu} - \mathbf{G}_{(\eta)} + \mathbf{D} \boldsymbol{\nu} + \boldsymbol{\tau} + \boldsymbol{\tau}_a), \quad (9)$$

where,

$$\boldsymbol{\nu} = [\mathbf{v}^T \ \dot{\phi}_L \ \dot{\theta}_L]^T,$$

$$\boldsymbol{\tau} = [(\mathbf{R}(\Theta) \mathbf{f})^T \ 0 \ 0]^T,$$

$$\boldsymbol{\tau}_a = [\mathbf{f}_e^T \ 0 \ 0]^T, \mathbf{f}_e \in \mathbb{R}^{3 \times 1},$$

$$\mathbf{D} = \text{diag}([0 \ 0 \ 0 \ d \ d]), d > 0,$$

$$\mathbf{G}_{(\eta)} = \begin{bmatrix} 0 \\ 0 \\ -g(m_L + m_c) \\ L g m_L \cos(\theta_L) \sin(\phi_L) \\ L g m_L \cos(\phi_L) \sin(\theta_L) \end{bmatrix}. \quad (10)$$

$M_{(\eta)}^*$ and $C_{(\eta,\nu)}^*$ are presented in detail in Appendix A, where $c\phi_L$, $s\phi_L$, $c\theta_L$, and $s\theta_L$ represent $\cos \phi_L$, $\sin \phi_L$, $\cos \theta_L$, and $\sin \theta_L$, respectively. The position and angular components are represented in the state vector $\boldsymbol{\eta} = [\mathbf{p} \ \phi_L \ \theta_L]^T$. The resulting nonlinear model considers a rigid tether between the UAV and the suspended load. Nevertheless, the tether is not rigid in real situations, and the approximation is valid for simplifying the modeling and analysis of the system. When the angle $\theta_L \geq 90^\circ$, the load will collide with the UAV. To avoid the singularity of $\cos(\theta_L)$ in $M_{(\eta)4,4}^*$ and $C_{(\eta,\nu)4,4}^*$, two product expressions are added to the dynamics, where ξ is an infinitesimal positive constant [10]:

$$M_{(\eta)4,4}^* = L^2 m_L \cos^2 \theta_L + \xi \sin^2 \theta_L, \quad (11)$$

$$C_{(\eta,\nu)4,4}^* = -\frac{1}{2} L^2 m_L \dot{\theta}_L \sin 2\theta_L + \frac{1}{2} \xi \dot{\theta}_L \sin 2\theta_L. \quad (12)$$

III. ROBUST CONTROL

This section details the performance specifications and the control design for the UAV with suspended load. The chosen methodology is robust control based on the \mathcal{H}_∞ norm.

The nonlinear model presented in (8) and (9), along with the UAV parameters for a suspended load provided in the case study [10] and listed in Table I, are utilized for linearization. The resulting matrices \mathbf{A} , \mathbf{B} , \mathbf{C} , and \mathbf{D} , detailed in Appendix B, were obtained from the linearization around an operating point using the *linmod* function in MATLAB. Specific details regarding the parameter values used are provided in the code (V).

$$\mathbf{G} : \left\{ \begin{array}{l} \dot{\mathbf{x}} = \mathbf{A}\mathbf{x} + \mathbf{B}\mathbf{u} \\ \mathbf{y} = \mathbf{C}\mathbf{x} + \mathbf{D}\mathbf{u}, \end{array} \right\}, \quad (13)$$

where \mathbf{x} is the state vector, \mathbf{u} is the control vector, and \mathbf{y} is the measurement output vector.

In this paper, a robust linear control \mathcal{H}_∞ was designed to

TABLE I
UAV PARAMETERS

Parameter	Description	Value	Unit
m_c	UAV mass	2.5	kg
m_L	Payload mass	0.2	kg
L	Suspension length	2	m
g	Gravity constant	9.8	m/s ²

guarantee good performance in autonomous trajectory tracking, as well as rejection of disturbances and sensor noise, according to [29]. Fig. 1 illustrates the structure of the robust control system in a two port diagram where \mathbf{G} from (13) represents the LTI system, embedded within the extended plant \mathbf{P} . The weighting functions denoted as W_S , W_T , and W_C , \mathbf{w} representing exogenous inputs and \mathbf{z} representing exogenous outputs.

The exogenous input vector (\mathbf{w}) includes the reference signal \mathbf{r} , and the exogenous output vector (\mathbf{z}) includes the error signal $\tilde{\mathbf{e}}$, the output error signal $\tilde{\mathbf{y}}$, and the control signal $\tilde{\mathbf{u}}$. The objective is to find the suboptimal controller \mathbf{K} that minimizes the norm of the transfer function between \mathbf{z} and \mathbf{w} using computational methods.

A. Weighting Functions

To specify performance and robustness in closed loop, weighting functions must be chosen according to [30]. In this work, we consider three weighting functions: W_S , W_T , and W_C .

The weighting function $W_S = \text{diag}[W_{Sx}W_{Sy}W_{Sz}]$ is applied to the linear velocities along the x , y , and z axes, respectively. This weighting function utilizes the sensitivity function $S = (I + KG)^{-1}$, which is related to good tracking performance and disturbance rejection.

$$W_S = \frac{s/M_s + \omega_{bs}}{s + \omega_{bs}\varepsilon_s}, \quad (14)$$

where M_s is the sensitivity function gain margin, ω_S is the closed-loop response bandwidth, and ε_s is a constant that represents a trade-off between sensitivity at low values and robustness as it increases.

The controller sensitivity function $C = KS$ is weighted by the weighting function $W_C = \text{diag}[W_{C1}W_{C2}W_{C3}]$, where KS limits the controller according to actuator specifications.

$$W_C = \frac{s + \omega_{bc}/M_c}{\varepsilon_c s + \omega_{bc}}, \quad (15)$$

where M_c is the magnitude of C , ω_{bc} is the bandwidth of the controller, and ε_c is a constant representing a trade-off between sensitivity and robustness, unlike ε_s . A smaller ε_c tends to increase sensitivity even further and may result in instability.

$T = (I - S)$ is a complementary sensitivity function from the weighting function W_T that is related to rejection of sensor noise [31].

$$W_T = \frac{s + \omega_{bt}/M_t}{s\varepsilon_t + \omega_{bt}}, \quad (16)$$

where ε_t is a constant, lower values imply that the system exhibits better reference tracking, while a higher value enhances robustness.

The control design needs the terms of the sensitivity functions S , C , and T to have the following characteristics: For S to reject disturbances, it requires a small value at low frequencies; T rejects noise from sensors with small values at high frequencies; and C increases the control efficiency by reducing controller effort, for which it needs small values at high frequencies. Based on the literature [32] and [30] and after numerical simulations, we found that the values W_S , W_T , and W_C that give us the best results for good performance of the controller are shown in Table II.

B. Control Synthesis

The application of the order reduction method, as described in [29], simplifies the dynamic model of the system and facilitates analysis, while preserving critical dynamics and stability properties.

After identifying which of the 10 state variables in (17) of the matrices \mathbf{A} , \mathbf{B} , \mathbf{C} , and \mathbf{D} have the least impact on the critical dynamics of the system, the 3 state variables that

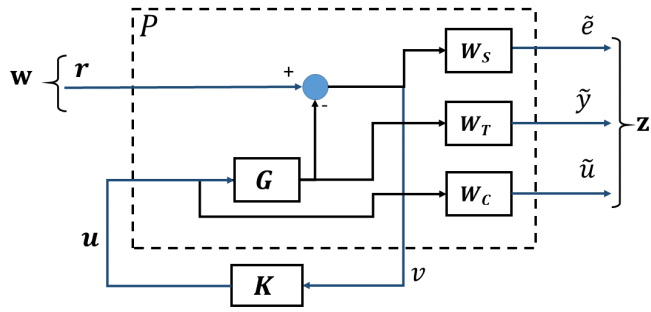
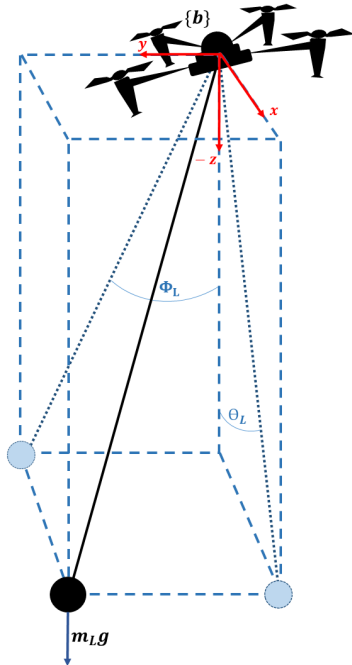


Fig. 1. Closed-loop extended plant and controller structure.

TABLE II
WEIGHTING FUNCTION VALUES

Weighting function	Parameter	Value
W_S	ω_{bsx}	$24 \cdot 10^{-3}$
	ω_{bsy}	$24 \cdot 10^{-3}$
	ω_{bsz}	$162 \cdot 10^{-3}$
	M_s	460
	ε_s	10^{-2}
W_C	ω_{bcx}	$8 \cdot 10^4$
	ω_{bcy}	$8 \cdot 10^4$
	ω_{bcz}	$9 \cdot 10^4$
	M_c	7800
	ε_c	10^{-2}
W_T	ω_{btx}	4590
	ω_{bty}	4590
	ω_{btz}	5100
	M_t	400
	ε_t	10^{-4}

Fig. 2. UAV illustration with load angles : ϕ_L and θ_L .

correspond to the positions x , y , and z of the UAV were

removed, resulting in the corresponding variables ν , ϕ_L , and θ_L , where these matrices (18) satisfy the conditions of observability and controllability.

$$\begin{array}{c|c} \mathbf{A}_{10 \times 10} & \mathbf{B}_{10 \times 3} \\ \hline \mathbf{C}_{3 \times 10} & \mathbf{D}_{3 \times 3} \end{array}, \quad (17)$$

$$\begin{array}{c|c} \mathbf{A}_{7 \times 7} & \mathbf{B}_{7 \times 3} \\ \hline \mathbf{C}_{3 \times 7} & \mathbf{D}_{3 \times 3} \end{array}. \quad (18)$$

Based on the aforementioned data, the Robust Control Toolbox in MATLAB computes $K(s)$ to find $\gamma \in \mathbb{R}$, which is associated with a suboptimal \mathcal{H}_∞ control problem.

For each value of γ , there exists a stabilizing controller such that the \mathcal{H}_∞ norm of the closed-loop transfer function between the disturbance input \mathbf{w} and the regulated output \mathbf{z} , represented as $T_{z\mathbf{w}}$ satisfies $\|T_{z\mathbf{w}}\|_\infty < \gamma$, indicating that the controller is stabilizing but may not be the globally optimal solution. To find the optimal controller, γ is iterated over a range of values until finding the smallest possible, γ_{\min} . Which represents the minimum bound on $\|T_{z\mathbf{w}}\|_\infty$ that ensures both stability and performance. Once the suboptimal solution has been identified, $T_{z\mathbf{w}}$ and $K(s)$ must satisfy the following expression:

$$\|T_{z\mathbf{w}}\|_\infty = \gamma, \quad (19)$$

The existence of a stabilizing controller $K(s)$ satisfies (19) if and only if the solution to the Riccati equations (20) and (21) has solutions $\mathbf{X} \geq 0$ and $\mathbf{Y} \geq 0$ respectively, and $K(s)$ has the same state number as the extended plant $P(s)$ [29], [33].

$$\mathbf{A}^T \mathbf{X}_\infty + \mathbf{X}_\infty \mathbf{A} + \mathbf{C}_1^T \mathbf{C}_1 + \mathbf{X}_\infty (\gamma^{-2} \mathbf{B}_1 \mathbf{B}_1^T - \mathbf{B}_2 \mathbf{B}_2^T) \mathbf{X}_\infty = 0, \quad (20)$$

such that: $\lambda_i[\mathbf{A} + (\gamma^{-2} \mathbf{B}_1 \mathbf{B}_1^T - \mathbf{B}_2 \mathbf{B}_2^T) \mathbf{X}_\infty] < 0, \forall i$.

$$\mathbf{A} \mathbf{Y}_\infty + \mathbf{Y}_\infty \mathbf{A}^T + \mathbf{B}_1 \mathbf{B}_1^T + \mathbf{Y}_\infty (\gamma^{-2} \mathbf{C}_1^T \mathbf{C}_1 - \mathbf{C}_2^T \mathbf{C}_2) \mathbf{Y}_\infty = 0, \quad (21)$$

such that: $\lambda_i[\mathbf{A} + \mathbf{Y}_\infty (\gamma^{-2} \mathbf{C}_1^T \mathbf{C}_1 - \mathbf{C}_2^T \mathbf{C}_2)] < 0, \forall i$, where λ_i are eigenvalues.

IV. RESULTS

The proposed controller is tested in a UAV simulator built in Simulink to analyze the \mathcal{H}_∞ controller implemented in a linear and nonlinear system under conditions similar to an actual scenario, an environment with disturbances caused by the forces of the air, represented by random noise in \mathbf{f}_e^T of τ_a . The tuning process found the γ of 0.00567 to guarantee the condition for a suboptimal \mathcal{H}_∞ design, given in (19).

A good robustness does not always suggest good performance; however, the results show that the controller performed well, achieving the reference velocity V_z in 2.6 seconds. Given the UAV's mass of 2.5 kg, as stated in the system parameters in Tab. I, the UAV performs better when m_c is lower.

A. Frequency Response

The suboptimal gamma value achieved is $\gamma = 0.00567$, and the controller variables K are reduced to 7 states.

Fig. 3 presents the three sensitivity responses S_1 , S_2 and S_3 , relative to the three velocities V_x , V_y , and V_z , respectively. S_1

presents low value at low frequencies with slope starting in 39.02 dB/dec without crossing its weighting given by $1/W_{S_1}$. S_2 presents low value at low frequencies with slope starting in 35.68 dB/dec and it does not cross $1/W_{S_2}$. S_3 presents a low value at low frequencies with a slope starting at 38.51 dB/dec, and it does not cross its weighting given by $1/W_{S_3}$ either.

Fig. 4 presents the three complementary sensitivity responses T_1 , T_2 , and T_3 , relative to the three velocities V_x , V_y , and V_z , respectively. T_1 presents a low value at high frequencies, with a slope starting at -39.99 dB/dec without crossing its weighting given by $1/W_{T_1}$. T_2 presents a low value at high frequencies with a slope starting in -40.01 dB/dec, and it does not cross $1/W_{T_2}$. T_3 presents a low value at high frequencies with a slope starting at -42.06 dB/dec, and it does not cross its weighting given by $1/W_{T_3}$ either.

Fig. 5 presents the \mathcal{H}_∞ norm, which is limited to values less than 1.

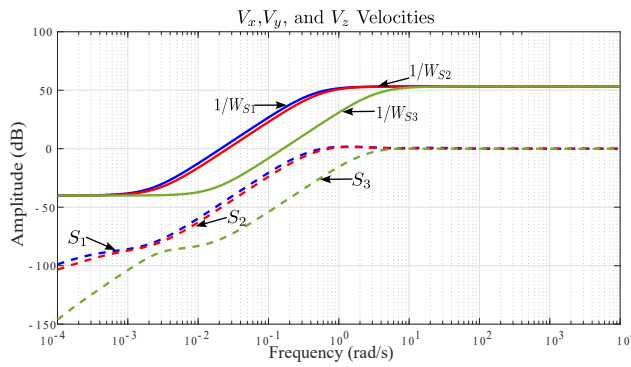


Fig. 3. Sensitivity function S_1, S_2, S_3 and Weighting inverse function $1/W_{S_1}, 1/W_{S_2},$ and $1/W_{S_3}$ for $V_{x,y,z}$.

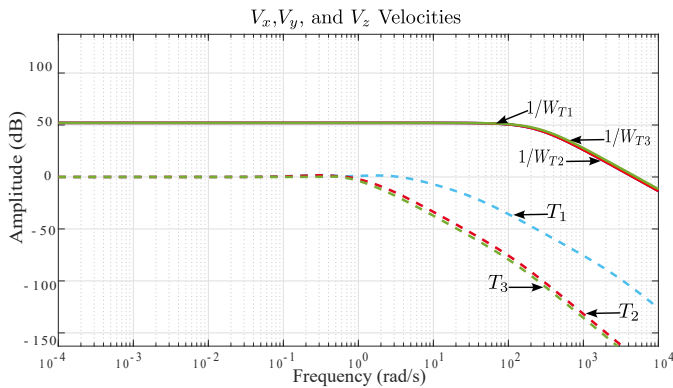


Fig. 4. Complementary Sensitivity $T_1, T_2,$ and T_3 and Weighting inverse function $1/W_{T_1}, 1/W_{T_2},$ and $1/W_{T_3}$ for $V_{x,y,z}$.

B. Time Response

1) *Linear Response:* Fig. 6 shows the velocity vector response $\mathbf{v} = [V_x, V_y, V_z]^T$ in $\{n\}$ and presents a good tracking with respect to the reference velocity vector, defined by $[V_{xr}, V_{yr}, V_{zr}]^T$. This reference velocity vector is composed of pulse signals of amplitude 5 m/s, a time width of 15 s, and rising edge times of 15 s, 20 s, and 25 s, respectively. The velocity V_x follows the reference V_{xr} with an overshoot of 1

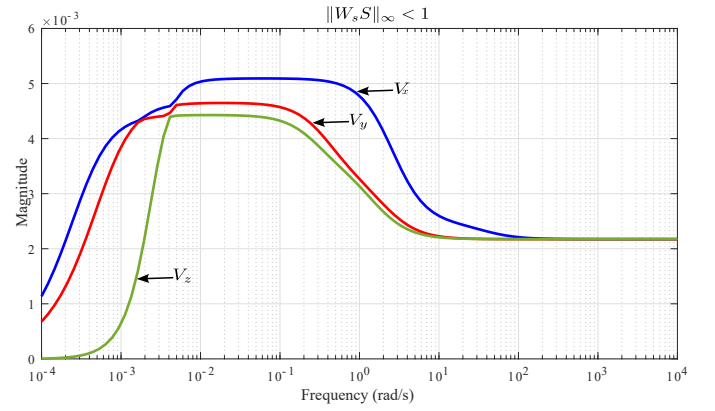


Fig. 5. Transfer Matrix $W_S S$.

m/s and a settling time of 35.2 s at $\pm 2\%$. The velocity V_y follows the reference V_{yr} with an overshoot of 1 m/s and a settling time of 37.7 s at $\pm 2\%$. The velocity V_z follows the reference V_{zr} with an overshoot of 0.8 m/s and a settling time of 17.7 s at $\pm 2\%$.

Fig. 7 shows the ϕ_L and θ_L responses that represent the locations of the suspended load when the same reference velocity vector $[V_{xr}, V_{yr}, V_{zr}]^T$ is applied to the UAV. When the rising edge happens in V_{zr} , ϕ_L and θ_L present a slight displacement of 0.58° and 0.59° , respectively, indicating a good disturbance rejection and keeping the load safe. When the rising edge happens in V_{xr} , ϕ_L maintains a slight displacement and θ_L decreases to reach a value of -67.6° at 25.5 s, converging to a constant value close to -60° . When the rising edge happens in V_{yr} , ϕ_L increases to reach a value of 68.4° at 29.9 s, converging to a constant value close to 60° , and θ_L keeps its behavior as described before. This maneuver is typical in load transportation where the UAV takes off from the ground, increases its velocity in the z direction to achieve the desired altitude, and then moves in the x and y coordinates. The results show good disturbance rejection, and the robust control guarantees limited displacements of the load, with $\phi_L < 70^\circ$ and $\theta_L < 70^\circ$.

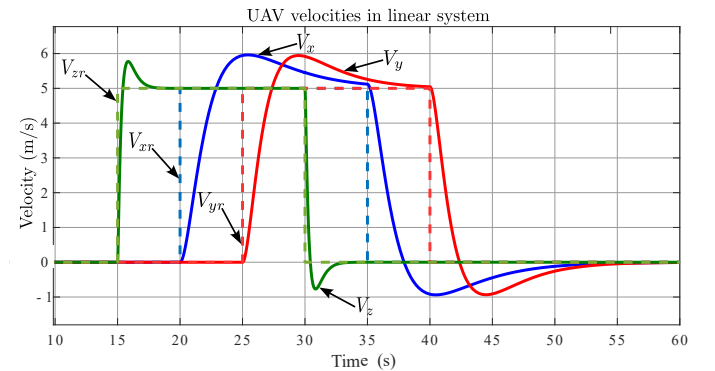


Fig. 6. Linear responses of velocities (V_x, V_y and V_z) to pulse reference velocities (V_{xr}, V_{yr} and V_{zr}).

2) *Nonlinear Response:* Fig. 8 shows the nonlinear responses of velocities considering the reference velocities, the same ones used in the previous analysis. The velocity V_x

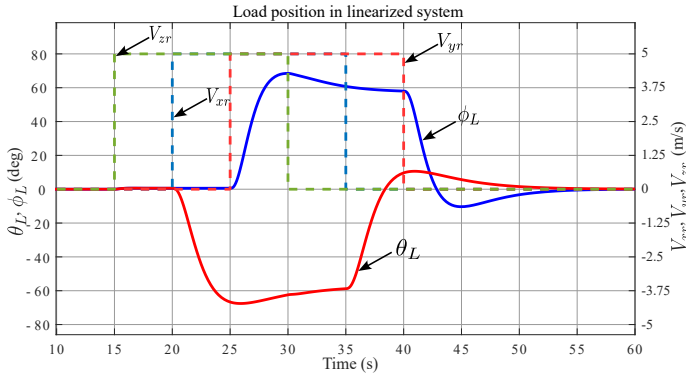


Fig. 7. Linear responses of ϕ_L and θ_L to pulse reference velocities (V_{xr} , V_{yr} and V_{zr}).

follows the reference V_{xr} with an overshoot of 1.001 m/s and has a settling time of 35.1 s at $\pm 2\%$. The velocity V_y follows the reference V_{yr} with an overshoot of 0.9 m/s and has a settling time of 37.7 s at $\pm 2\%$. The velocity V_z follows the reference V_{zr} with an overshoot of 0.83 m/s and has a settling time of 17.6 s at $\pm 2\%$.

Fig. 9 shows the ϕ_L and θ_L nonlinear responses that represent the locations of the suspended load when the reference velocity vector $[V_{xr}, V_{yr}, V_{zr}]^T$ is applied to the UAV. When the rising edge happens in V_{zr} , ϕ_L and θ_L do not present variations in the displacement, indicating better performance compared to the linear responses. When the rising edge happens in V_{xr} , ϕ_L does not present variations in its displacement, and θ_L decreases to reach a value of -13.9° at 21.7 s, converging to a constant value close to 0° . When the rising edge happens in V_{yr} , ϕ_L increases to reach a value of 16.5° at 26.6 s, converging to a constant value close to 0° , and θ_L keeps its behavior as described before. The current \mathcal{H}_∞ controller improves the performance of the suspended load transportation in which the response presents less oscillation amplitude and converges quickly to the equilibrium point. The load angular displacements, ϕ_L and θ_L , reach maximum amplitudes of 16.5° and 13.9° , respectively. Both angles converge quickly to 0° despite the pulse reference velocities being applied to the UAV. These results evidence a better performance of the controller compared to the simulation results presented in [27], where the load angular displacements, ϕ_L and θ_L , reach maximum amplitudes of 50° and 20° , respectively. In other similar research [34], the \mathcal{H}_∞ linear control was also used in a UAV with 2 mobile thrusts, which can have oscillatory behaviors within 40° , greater than the results achieved in this work (less than 20°).

In [35], a \mathcal{H}_∞ controller is used in a linearized model based on Euler-Lagrange with 0.55 kg mass of the UAV and 0.05 kg mass of the suspended load, and the pendulum oscillation achieved peaks of 20° . In this research, we presented the application of a \mathcal{H}_∞ control for the model based on the Kane equation and achieved better results than the last work based on the Euler-Lagrange modeling. These new results, in comparison with this last investigation, are encouraging since the peak oscillation is reduced to 16.5° , considering a heavier UAV with 2.5 kg mass and a suspended load of 0.2

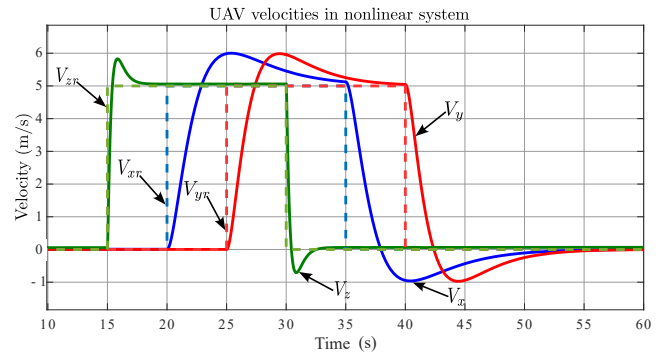


Fig. 8. Nonlinear responses of velocities (V_x , V_y and V_z) to pulse reference velocities (V_{xr} , V_{yr} and V_{zr}).

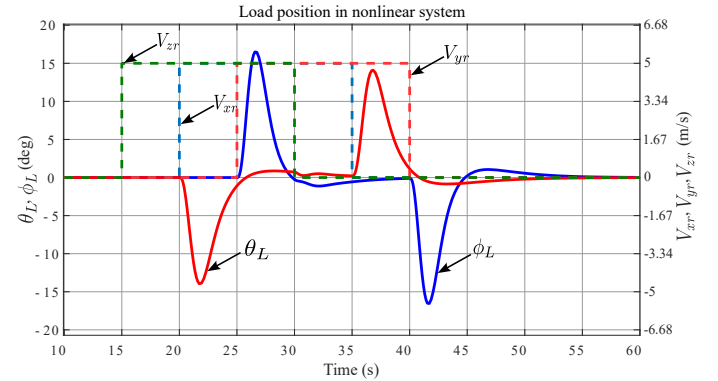


Fig. 9. Nonlinear responses of ϕ_L and θ_L to pulse reference velocities (V_{xr} , V_{yr} and V_{zr}).

kg mass. Moreover, the suspended load is transported with good performance, keeping stable and steady state motion when the UAV is moving at constant velocities up to 5 m/s. In the simulations, it was observed that the controller synthesis is sensitive to changes in m_L , which should be considered in future implementations. Regarding the feasibility of implementing this type of controller, works such as [31] present control of a six-degree-of-freedom system using an LPC2148 microcontroller with a 32-bit ARM7 processor.

V. CONCLUSION

This paper proposes a \mathcal{H}_∞ mixed sensitivity approach applied to the system of a UAV with a suspended load, connected by a link to the UAV's CG. This highly coupled system is modeled using Kane's equations, assuming that the link is rigid. Building upon this model, the computational simulation shows that the frequency domain response, corresponding to a sub-optimal γ of 0.00567, ensures better performance and stability against system disturbances, environmental perturbations, and sensor noise. Furthermore, the time domain response demonstrates the system's convergence to the reference velocity, with angular swings below 20° and stabilizing quickly when the controller is applied to the nonlinear system, which closely resembles the real system. These results demonstrate an improvement over similar studies, such as those in [8], [27]. In summary, it is demonstrated that the proposed robust controller is a good alternative for enhancing performance in the

transportation of suspended loads using UAVs in applications where there are disturbances from different sources. As part of the project, we plan to test the effectiveness of the proposed controller in future work by implementing it in a real system using the DJI-F450 quadrotor.

ACKNOWLEDGMENTS

This work was carried out thanks to the Laboratory for Control of Complex Processes and Unmanned Vehicles, where this research was developed. An initial version of this work was published as a preprint [36]. The Matlab programming codes can be accessed at doi.org/10.5281/zenodo.10886927.

REFERENCES

- [1] V. San Juan, M. Santos, and J. M. Andújar, "Intelligent uav map generation and discrete path planning for search and rescue operations," *Complexity*, vol. 2018, no. 1, Jan. 2018, DOI: 10.1155/2018/6879419.
- [2] A. Madridano, S. Campos, A. Al-Kaff, F. García, D. Martín, and A. Escalera, "Vehículo aéreo no tripulado para vigilancia y monitorización de incendios," *Revista Iberoamericana de Automática e Informática industrial*, vol. 17, no. 3, p. 254, Jul. 2020, DOI:10.4995/riai.2020.11806.
- [3] A. J. Moore, M. Schubert, N. Rymer, S. Balachandran, M. Consiglio, C. Munoz, J. Smith, D. Lewis, and P. Schneide, "Inspection of electrical transmission structures with uav path conformance and lidar-based geofences," in *2018 IEEE Power amp; Energy Society Innovative Smart Grid Technologies Conference (ISGT)*. Washington, DC, USA: IEEE, 2018, pp. 1–5, DOI:10.1109/isgt.2018.8403395.
- [4] Q. Shi, D. Liu, H. Mao, B. Shen, and M. Li, "Wind-induced response of rice under the action of the downwash flow field of a multi-rotor uav," *Biosystems Engineering*, vol. 203, pp. 60–69, Mar. 2021, DOI:10.1016/j.biosystemseng.2020.12.012.
- [5] E. Nogueira, B. Oliveira, R. Bulcão-Neto, and F. Soares, "A systematic review of the literature on machine learning methods applied to high throughput phenotyping in agricultural production," *IEEE Latin America Transactions*, vol. 21, no. 7, pp. 783–796, 2023, DOI:10.1109/TLA.2023.10244177.
- [6] J. J. Potter, C. J. Adams, and W. Singhose, "A planar experimental remote-controlled helicopter with a suspended load," *IEEE/ASME Transactions on Mechatronics*, vol. 20, no. 5, pp. 2496–2503, Oct. 2015, DOI:10.1109/tmech.2014.2386801.
- [7] B. Li, Y. Li, P. Yang, and X. Zhu, "Adaptive neural network-based fault-tolerant control for quadrotor-slung-load system under marine scene," *IEEE Transactions on Intelligent Vehicles*, vol. 9, no. 1, pp. 681–691, 2024, DOI:10.1109/TIV.2023.3333888.
- [8] K. Y. Us, A. Cevher, M. Sever, and A. Kırılı, "On the effect of slung load on quadrotor performance," *Procedia Computer Science*, vol. 158, pp. 346–354, 2019, DOI:10.1016/j.procs.2019.09.061.
- [9] M. Bernard and K. Kondak, "Generic slung load transportation system using small size helicopters," in *2009 IEEE International Conference on Robotics and Automation*. Kobe, Japan: IEEE, 2009, DOI:10.1109/ROBOT.2009.5152382.
- [10] K. Klausen, T. I. Fossen, and T. A. Johansen, "Nonlinear control of a multirotor uav with suspended load," in *2015 International Conference on Unmanned Aircraft Systems (ICUAS)*. Denver, CO, USA: IEEE, 2015, DOI:10.1109/icuas.2015.7152289.
- [11] W. Eikyu, K. Sekiguchi, and K. Nonaka, "Nonlinear control for the extended model of the load-suspended uav based on the experiments," *IFAC-PapersOnLine*, vol. 54, no. 14, pp. 90–95, 2021, DOI:10.1016/j.ifacol.2021.10.334.
- [12] J. E. Sierra-García and M. Santos, "Intelligent control of an uav with a cable-suspended load using a neural network estimator," *Expert Systems with Applications*, vol. 183, p. 115380, Nov. 2021, DOI:10.1016/j.eswa.2021.115380.
- [13] R. A. Barrón-Gómez, L. E. Ramos-Velasco, E. S. Espinoza Quesada, and L. R. García Carrillo, "Wavelet neural network pid controller for a uas transporting a cable-suspended load," *IFAC-PapersOnLine*, vol. 50, no. 1, pp. 2335–2340, Jul. 2017, DOI:10.1016/j.ifacol.2017.08.419.
- [14] L. Alves Fagundes-Junior, A. Fialho Coelho, D. Khede Dourado Villa, M. Sarcinelli-Filho, and A. Santos Brandão, "Communication delay in uav missions: A controller gain analysis to improve flight stability," *IEEE Latin America Transactions*, vol. 21, no. 1, pp. 7–15, 2023, DOI:10.1109/TLA.2023.10015140.
- [15] A. Erasmus and H. Jordaan, "Robust adaptive control of a multirotor with an unknown suspended payload," *IFAC-PapersOnLine*, vol. 53, no. 2, pp. 9432–9439, 2020, DOI:10.1016/j.ifacol.2020.12.2414.
- [16] S. Yang, B. Xian, J. Cai, and G. Wang, "Finite-time convergence control for a quadrotor unmanned aerial vehicle with a slung load," *IEEE Transactions on Industrial Informatics*, vol. 20, no. 1, pp. 605–614, 2024, DOI:10.1109/TII.2023.3268762.
- [17] C. Peris, M. Norton, and S. Y. Khoo, "Adaptive multi surface sliding mode control of a quadrotor slung load system," *2024 10th International Conference on Automation, Robotics and Applications (ICARA)*, 2024, DOI:10.1109/ICARA60736.2024.10552970.
- [18] X. Lan, L. Gong, L. Zheng, S. Liu, and W. Xu, "Anti-swing strategy of a quadrotor with suspended payload based on model predictive control," *2023 9th International Conference on Control Science and Systems Engineering (ICCSSE)*, 2023, DOI:10.1109/ICCSSE59359.2023.10245849.
- [19] F. Panetsos, G. C. Karras, and K. J. Kyriakopoulos, "An nmpc framework for tracking and releasing a cable-suspended load to a ground target using a multirotor uav," *2024 IEEE International Conference on Robotics and Automation (ICRA)*, vol. 50, pp. 10057–10063, 2024, DOI:10.1109/ICRA57147.2024.10610034.
- [20] N. Urbina-Brito, M.-E. Guerrero-Sánchez, G. Valencia-Palomo, O. Hernández-González, F.-R. López-Estrada, and J. A. Hoyo-Montaño, "A predictive control strategy for aerial payload transportation with an unmanned aerial vehicle," *Mathematics*, vol. 9, no. 15, p. 1822, Aug. 2021, DOI: 10.3390/math9151822.
- [21] M. E. Guerrero-Sánchez, O. Hernández-González, G. Valencia-Palomo, D. A. Mercado-Ravell, F. R. López-Estrada, and J. A. Hoyo-Montaño, "Robust ida-pbc for under-actuated systems with inertia matrix dependent of the unactuated coordinates: application to a uav carrying a load," *Nonlinear Dynamics*, vol. 105, no. 4, pp. 3225–3238, Aug. 2021, DOI:10.1007/s11071-021-06776-7.
- [22] M.-E. Guerrero-Sánchez, O. Hernández-González, R. Lozano, C.-D. García-Beltrán, G. Valencia-Palomo, and F.-R. López-Estrada, "Energy-based control and lmi-based control for a quadrotor transporting a payload," *Mathematics*, vol. 7, no. 11, p. 1090, Nov. 2019, DOI:10.3390/math7111090.
- [23] H. Wang, Z. Li, H. Xiong, and X. Nian, "Robust h_{∞} attitude tracking control of a quadrotor uav on so(3) via variation-based linearization and interval matrix approach," *ISA Transactions*, vol. 87, pp. 10–16, Apr. 2019, DOI:10.1016/j.isatra.2018.11.015.
- [24] H. M. Omar, R. Akram, S. M. Mukras, and A. A. Mahvouz, "Recent advances and challenges in controlling quadrotors with suspended loads," *Alexandria Engineering Journal*, vol. 63, pp. 253–270, Jan. 2023, DOI:10.1016/j.aej.2022.08.001.
- [25] O. Hernández-González, B. Targui, G. Valencia-Palomo, and M. Guerrero-Sánchez, "Robust cascade observer for a disturbance unmanned aerial vehicle carrying a load under multiple time-varying delays and uncertainties," *International Journal of Systems Science*, vol. 55, no. 5, pp. 1056–1072, Jan. 2024, DOI:10.1080/00207721.2023.2301496.
- [26] R. Mahony, V. Kumar, and P. Corke, "Multirotor aerial vehicles: Modeling, estimation, and control of quadrotor," *IEEE Robotics amp; Automation Magazine*, vol. 19, no. 3, pp. 20–32, Sep. 2012, DOI:10.1109/mra.2012.2206474.
- [27] K. Klausen, T. I. Fossen, and T. A. Johansen, "Nonlinear control with swing damping of a multirotor uav with suspended load," *Journal of Intelligent amp; Robotic Systems*, vol. 88, no. 2–4, pp. 379–394, Mar. 2017, DOI:10.1007/s10846-017-0509-6.
- [28] M. Bernard, K. Kondak, I. Maza, and A. Ollero, "Autonomous transportation and deployment with aerial robots for search and rescue missions," *Journal of Field Robotics*, vol. 28, no. 6, pp. 914–931, Oct. 2011, DOI:10.1002/rob.20401.
- [29] S. Skogestad and I. Postlethwaite, *Multivariable feedback control*, 2nd ed. Chichester: Wiley, 2010.
- [30] K. Zhou and J. C. Doyle, *Essentials of robust control*, ser. Prentice Hall international editions, P. Hall, Ed. Upper Saddle River, NJ: Tom Robbins, 1998, includes bibliographical references and index.
- [31] J. C. Cutipa-Luque, D. C. Donha, J. L. D. Dantas, L. M. de Oliveira, and E. A. de Barros, "Robust control of an underactuated auv," *IFAC Proceedings Volumes*, vol. 45, no. 27, pp. 138–143, 2012, DOI:10.3182/20120919-3-IT-2046.00024.

- [32] M. M. Huayna-Aguilar, J. C., and P. Raul, "Robust control and fuzzy logic guidance for an unmanned surface vehicle," *International Journal of Advanced Computer Science and Applications*, vol. 11, no. 8, 2020, DOI:10.14569/IJACSA.2020.0110894.
- [33] J. Doyle, K. Glover, P. Khargonekar, and B. Francis, "State-space solutions to standard h_2 and h_∞ control problems," *IEEE Transactions on Automatic Control*, vol. 34, no. 8, pp. 831–847, 1989, DOI:10.1109/9.29425.
- [34] G. V. Raffo and M. M. d. Almeida, "A load transportation nonlinear control strategy using a tilt-rotor uav," *Journal of Advanced Transportation*, vol. 2018, pp. 1–20, Jun. 2018, DOI:10.1155/2018/1467040.
- [35] M. Guo, Y. Su, and D. Gu, "Mixed h_2 / h_∞ tracking control with constraints for single quadcopter carrying a cable-suspended payload," *IFAC-PapersOnLine*, vol. 50, no. 1, pp. 4869–4874, Jul. 2017, DOI:10.1016/j.ifacol.2017.08.976.
- [36] J. A. Enriquez, T. Y. Galarza, J. C. Cutipa, and D. P. Ferruzo, "Robust control of an rotary-wing uav with suspended load," *Research Square Platform LLC*, Nov. 2023, DOI:10.21203/rs.3.rs-3403704/v1.



Jefferson Abraham Enriquez Quispe received the bachelor degree in electronic engineering from the Universidad Nacional de San Agustín de Arequipa, Peru, in 2021. His research interests include advanced control systems for unmanned aerial vehicles (AUVs), and electric vehicles.



Tito Yvan Galarza Delgado received the degree in electronic engineering in 2002 and the M.Sc. degree in Telecommunications Engineering in 2022 from the Universidad Nacional de San Agustín de Arequipa, Peru. He is currently a designated worker in the networks and telecommunications area of the Information Technology Office of the Universidad Nacional de San Agustín de Arequipa. He is also a teacher in the postgraduate unit of the Universidad Católica San Pablo, instructor trainer of the CISCO Network Academy, and specialist teacher in information technology at the CIBERTEC Institute.



Juan C. Cutipa Luque received the degree in electronic engineering from the Universidad Nacional de San Agustín de Arequipa, Peru, in 2004, and the M.Sc. and Ph.D. degrees in mechanical engineering from the University of São Paulo, Brazil, in 2007 and 2012, respectively. He is currently a Professor with the Electronic Engineering Department, Universidad Nacional de San Agustín de Arequipa. His research interests include advanced control systems for autonomous underwater vehicles (AUVs), remote-operated submersible vehicles (ROVs), unmanned surface vehicles (USV), and electric vehicles.

APPENDIX A

$$\mathbf{M}_{(\eta)}^* = \begin{bmatrix} m_L + m_c & 0 & 0 & 0 & Lm_L c \theta_L \\ 0 & m_L & 0 & -Lm_L c \phi_L c \theta_L & Lm_L s \phi_L s \theta_L \\ 0 & 0 & m_L + m_c & -Lm_L c \theta_L s \phi_L & -Lm_L c \phi_L s \theta_L \\ 0 & -Lm_L c \phi_L c \theta_L & -Lm_L c \theta_L s \phi_L & L^2 m_L c \theta_L & 0 \\ Lm_L c \theta & Lm_L s \phi_L s \theta_L & -Lm_L c \phi_L c \theta_L & 0 & L^2 m_L \end{bmatrix}, \quad (22)$$

$$\mathbf{C}_{(\eta, \nu)}^* = \begin{bmatrix} 0 & 0 & 0 & 0 & -L\dot{\theta}_L m_L s \theta_L \\ 0 & 0 & 0 & Lm_L(\dot{\phi}_L c \theta_L s \phi_L + \dot{\theta}_L c \phi_L s \theta_L) & Lm_L(\dot{\phi}_L c \phi_L s \theta_L + \dot{\theta}_L c \theta_L s \phi_L) \\ 0 & 0 & 0 & -Lm_L(\dot{\phi}_L c \phi_L c \theta_L - \dot{\theta}_L s \phi_L s \theta_L) & -Lm_L(\dot{\theta}_L c \phi_L c \theta_L - \dot{\phi}_L s \phi_L s \theta_L) \\ 0 & 0 & 0 & -\frac{1}{2}L^2 \dot{\theta}_L m_L s(2\theta_L) & -\frac{1}{2}L^2 \dot{\phi}_L m_L s(2\theta_L) \\ 0 & 0 & 0 & \frac{1}{2}L^2 \dot{\phi}_L m_L s(2\theta_L) & 0 \end{bmatrix}, \quad (23)$$

APPENDIX B

$$\mathbf{A} = \begin{bmatrix} 0 & 0 & 0 & 0 & 0 & 1 & 0 & 0 & 0 & 0 \\ 0 & 0 & 0 & 0 & 0 & 0 & 1 & 0 & 0 & 0 \\ 0 & 0 & 0 & 0 & 0 & 0 & 0 & 1 & 0 & 0 \\ 0 & 0 & 0 & 0 & 0 & 0 & 0 & 0 & 1 & 0 \\ 0 & 0 & 0 & 0 & 0 & 0 & 0 & 0 & 0 & 1 \\ 0 & 0 & 0 & 3 \cdot 10^{-9} & -10^{-5} & 0 & 0 & 0 & 3 \cdot 10^{-5} & 0.4 \\ 0 & 0 & 0 & 5 \cdot 10^{-5} & 9 \cdot 10^{-9} & 0 & 0 & 0 & -0.4 & 10^{-5} \\ 0 & 0 & 0 & -4 \cdot 10^{-3} & -4 \cdot 10^{-3} & 0 & 0 & 0 & -10^{-3} & -10^{-3} \\ 0 & 0 & 0 & 2 \cdot 10^{-6} & -3 \cdot 10^{-4} & 0 & 0 & 0 & -2.7 & 2 \cdot 10^{-4} \\ 0 & 0 & 0 & -2 \cdot 10^{-9} & -10^{-4} & 0 & 0 & 0 & -2 \cdot 10^{-4} & -2.7 \end{bmatrix} \quad (24)$$

$$\mathbf{B} = \begin{bmatrix} 0 & 0 & 0 \\ 0 & 0 & 0 \\ 0 & 0 & 0 \\ 0 & 0 & 0 \\ 0 & 0 & 0 \\ 3.9 \cdot 10^{-1} & 2.9 \cdot 10^{-6} & -2.9 \cdot 10^{-4} \\ 2.9 \cdot 10^{-6} & 3.9 \cdot 10^{-1} & 2.9 \cdot 10^{-4} \\ -2.9 \cdot 10^{-4} & 2.9 \cdot 10^{-4} & 3.7 \cdot 10^{-1} \\ 0 & 0.2 & 0.2 \cdot 10^{-2} \\ -1.9 \cdot 10^{-1} & -1.9 \cdot 10^{-5} & 1.9 \cdot 10^{-3} \end{bmatrix}, \quad (25)$$

$$\mathbf{C} = \begin{bmatrix} 0 & 0 & 1 & 0 & 0 & 0 & 0 \\ 0 & 0 & 0 & 1 & 0 & 0 & 0 \\ 0 & 0 & 0 & 0 & 1 & 0 & 0 \end{bmatrix}, \quad (26)$$

$$\mathbf{D} = \begin{bmatrix} 0 & 0 & 0 \\ 0 & 0 & 0 \\ 0 & 0 & 0 \end{bmatrix}, \quad (27)$$